Title: LES-CMC simulations of different auto-ignition regimes of hydrogen in a hot turbulent air co-flow

Authors: I. Stankovic, E. Mastorakos and B. Merci

In: Flow, Turbulence and Combustion

I. Stankovic, E. Mastorakos and B. Merci (2013). LES-CMC simulations of different auto-ignition regimes of hydrogen in a hot turbulent air co-flow. Flow, Turbulence and Combustion. 90:583-604. DOI: 10.1007/s10494-013-9443-2

Noname manuscript No.
(will be inserted by the editor)

LES-CMC simulations of different auto-ignition regimes of hydrogen in a hot turbulent air co-flow

I. Stanković · E. Mastorakos · B. Merci

Received: date / Accepted: date

Abstract Large-Eddy Simulation (LES) results in combination with first-order Conditional Moment Closure (CMC) are presented for a hydrogen jet, diluted with nitrogen, issued into a turbulent co-flowing hot air stream. The fuel mixes with the co-flow air, ignites and forms a lifted-like flame. Global trends in the experimental observations are in general well reproduced: the auto-ignition length decreases with increase in co-flow temperature and increases with increase in co-flow velocity. In the experiments, the co-flow temperature was varied, so that different auto-ignition regimes, including low Damköhler number situations, were obtained (no ignition, random spots, flashback and lifted flame). All regimes are recovered in the simulations. Auto-ignition is found to be the stabilizing mechanism. The impact of different detailed chemistry mechanisms on the auto-ignition predictions is discussed. With increasing air temperature, the differences between the mechanisms considered diminish. The evolution of temperature, H_2O, H, HO_2 and OH from inert to burning conditions is discussed in mixture fraction space.

Keywords CMC · LES · auto-ignition · hydrogen chemistry

1 Introduction

Auto-ignition in turbulent non-premixed flows has significant practical applications and quite subtle fundamental aspects [1]. In numerical studies of auto-ignition phenomena, turbulence and unsteady chemistry must be modelled accurately. In order to obtain accurate simulation results for the turbulence, the Large-Eddy

I. Stanković · B. Merci
Department of Flow, Heat and Combustion Mechanics, Ghent University,
St.-Pietersnieuwstraat 41, 9000 Ghent Belgium
Tel.: +32 9 264 33 00
Fax: +32 9 264 35 75
E-mail: Ivana.Stankovic@UGent.be

E. Mastorakos
Hopkinson Laboratory, Engineering Department, Cambridge University, Trumpington Street, Cambridge, CB2 1PZ, United Kingdom

Simulation (LES) approach is gaining interest. For the turbulence-chemistry interaction, the Conditional Moment Closure (CMC) [2], Probability Density Function (PDF) [3], steady [4] and unsteady flamelet models [5] with presumed PDF or the flamelet/progress variable (FPV) or Flamelet Generated Manifold (FGM) model [6, 7] can be used. In this work we adopt the CMC approach, which can deal with slow chemistry, while it is in general less time consuming than PDF methods.

Previous LES studies, mostly focus on simple geometries such as the jet in vitiated air [8] or the fuel jet in heated air enclosed in a duct [9]. The focus of the present work is the latter test case. In [9], different set-ups are described. Here, we focus on auto-ignition in the case where the fuel jet velocity u_{fuel} is higher than the co-flow air velocity u_{cf}.

For validation purposes, the case of [8], for which more data are available, is in principle better suited and we briefly mention some basic results for this case. A more detailed analysis for this case will be reported later. Yet, the CMC code has already been extensively validated in e.g. [11–13], so that we consider it justified to focus here on [9]. This test case concerns auto-ignition of hot hydrogen, diluted with nitrogen, injected from a central nozzle into a heated turbulent air co-flow. In the experiment, visual observations over a wide range of operating conditions revealed qualitatively distinct regimes (no ignition, random spots, flashback and lifted flame). We illustrate below that all these regimes are encountered with our LES-CMC approach. The Berkeley and Sydney flame [8, 10] shows a continuous sheet, with only the base having a fragmented nature - see the images in [14, 15]. The Cambridge burner for some conditions shows a lifted or attached flame, but in others it shows a fragmented flame ('spots') everywhere. Our work aims to examine if both auto-ignition behaviours can be predicted by the same combustion model implemented in LES. LES has the intrinsic capability to capture unsteady flow features, which should be the key to simulating the transient auto-ignition spot behaviour.

Numerical investigations of the case [9], reported so far, were undertaken mainly with the transported PDF with detailed combustion model [16, 17], or tabulated chemistry [18] in combination with LES. In [19], the CMC model has been applied in a RANS context but the 'random spots' regime was not reproduced: in all cases studied an attached flame was formed. More recently, CMC has been successfully applied in LES context [20]. In all studies mentioned, the focus was on auto-ignition in the case of equal fuel and air velocities. As mentioned, we focus on case where $u_{fuel} > u_{cf}$.

At the relatively low temperatures, for the test case at hand, there is some uncertainty in the reaction rate constants and the choice of the detailed chemistry mechanism can be of great importance. Crucial are intermediates and slow reactions, which increase the pool of reactants. Therefore, the low temperature non-premixed auto-ignition behavior of the following chemistry mechanisms is discussed in [21]: Li et al. [22], Mueller et al. [23], Yetter et al. [24], O'Conaire et al. [25] and Konnov [26]. In the present paper, we compare only the mechanisms of [22–24] in 3D LES-CMC simulations. The sensitivity of RANS-PDF predictions of the auto-igniting jet in vitiated air [8] to the detailed hydrogen mechanism has already been reported [27–29]. The test case of [8] differs from [9] in composition of the fuel and co-flow, as well as in geometry and temperatures (e.g. T_{fuel}). Therefore, it is not straightforward to simply extrapolate the findings for case of [8] to the case of [9], studied here. This is reported in [21].

We have already reported LES-CMC results for this case [13]. There, we discussed various implementation options for the CMC combustion model in LES, the influence of the CFD and CMC mesh resolution in physical space and the turbulence inlet boundary conditions. These aspects are not repeated here and we take advantage of knowledge as reported in [13]. However, here we discuss 'random spots' regime and we illustrate that the first-order CMC, coupled with LES, is viable for the test case at hand, simulating different auto-ignition regimes of [9]. The scalar dissipation rate profiles are examined as well. Also, more detail sensitivity study of the lift-off height to different co-flow temperatures and velocities is reported for different chemistry mechanism.

2 LES-CMC modelling

The filtered mass and momentum equations are solved [30]:

$$\frac{\partial \bar{\rho}}{\partial t} + \frac{\partial (\bar{\rho}\widetilde{u}_i)}{\partial x_i} = 0 \tag{1}$$

$$\frac{\partial (\bar{\rho}\widetilde{u}_i)}{\partial t} + \frac{\partial (\bar{\rho}\widetilde{u}_i\widetilde{u}_j)}{\partial x_j} = -\frac{\partial \bar{p}}{\partial x_i} + \frac{\partial \widetilde{\tau}_{ij}}{\partial x_j} - \frac{\partial \tau_{ij}^{sgs}}{\partial x_j} \tag{2}$$

where $\bar{\rho}$ is the resolved density, $\widetilde{u}_i$ is the resolved velocity in the i direction, $\widetilde{\tau}_{ij} = \bar{\mu}\left(\frac{\partial \widetilde{u}_i}{\partial x_j} + \frac{\partial \widetilde{u}_j}{\partial x_i} - \frac{2}{3}\frac{\partial \widetilde{u}_k}{\partial x_k}\delta_{ij}\right)$ is the resolved stress tensor. $\tau_{ij}^{sgs} = \bar{\rho}(\widetilde{u_i u_j} - \widetilde{u}_i\widetilde{u}_j)$ is the sub-grid scale stress tensor, for which we apply the standard Smagorinsky model [31], with fixed model constant, $C_s = 0.1$ as in [13].

In [13], we illustrated that this is a justified choice for the test case at hand.

A transport equation for the filtered mixture fraction, $\widetilde{\xi}$ is also solved [13], where a constant Schmidt number ($Sc = Sc_t = 0.7$) has been considered.

The mixture fraction variance is obtained from a gradient type model [32,33]:

$$\widetilde{\xi''^2} = C\Delta^2 \frac{\partial \widetilde{\xi}}{\partial x_k}\frac{\partial \widetilde{\xi}}{\partial x_k} \tag{3}$$

where C is taken constant ($C = 0.1$) [13].

The CMC equations for the conditionally filtered reactive scalars in LES context read [34]:

$$\frac{\partial Q_\alpha}{\partial t} + \underbrace{\widetilde{u_i|\eta}\frac{\partial Q_\alpha}{\partial x_i}}_{T_1} - \underbrace{\widetilde{N|\eta}\frac{\partial^2 Q_\alpha}{\partial \eta^2}}_{T_2} = \underbrace{\widetilde{W_\alpha|\eta}}_{T_3} + \underbrace{\frac{1}{\overline{\rho}\widetilde{P}(\eta)}\frac{\partial}{\partial x_i}\left[\overline{\rho}\widetilde{P}(\eta)D_t\frac{\partial Q_\alpha}{\partial x_i}\right]}_{T_4} \tag{4}$$

$$\frac{\partial Q_T}{\partial t} + \underbrace{\widetilde{u_i|\eta}\frac{\partial Q_T}{\partial x_i}}_{T_1} - \underbrace{\widetilde{N|\eta}\left[\frac{1}{c_{p_\eta}}\left(\frac{\partial c_{p_\eta}}{\partial \eta} + \sum_{\alpha=1}^{n} c_{p,\alpha_\eta}\frac{\partial Q_\alpha}{\partial \eta}\right)\frac{\partial Q_T}{\partial \eta} + \frac{\partial^2 Q_T}{\partial \eta^2}\right]}_{T_2} =$$

$$\underbrace{-\frac{1}{c_{p_\eta}}\sum_{\alpha=1}^{n} h_\alpha\widetilde{W_\alpha|\eta}}_{T_3} + \underbrace{\frac{1}{\overline{\rho}\widetilde{P}(\eta)}\frac{\partial}{\partial x_i}\left[\overline{\rho}\widetilde{P}(\eta)D_t\frac{\partial Q_T}{\partial x_i}\right]}_{T_4} \tag{5}$$

where $Q_\alpha = \widetilde{Y_\alpha|\eta}$ represents the conditionally filtered reactive scalar, $\widetilde{u_i|\eta}$ is the conditionally filtered velocity, $\widetilde{N|\eta}$ is the conditionally filtered scalar dissipation rate and D_t is the sub-grid scale turbulent diffusivity. The variable η is the sample space variable for mixture fraction, ξ, and the operator $\cdot|\eta$ denotes fulfilment of the condition on the right hand side of the vertical bar. The conditional fluctuations around the conditional mean are neglected in the first order CMC.

The first term on the left-hand side of Eq. (4) is the unsteady term. The second term represents the transport by convection (T_1). The last term on the left-hand (T_2) side represents diffusion in mixture fraction space, also known as the conditional scalar dissipation rate term. The first term on the right-hand side (T_3) is the conditional chemical source term, determined using first order closure. The last term on the right-hand side, i.e. the sub-grid scale conditional flux, (term T_4). It accounts for the conditional transport in physical space and it is modelled using the gradient approach [13].

For complete closure of Eqs. (4) and (5), models are required for $\widetilde{N|\eta}$ and $\widetilde{u_i|\eta}$ as well. The conditionally filtered velocity is taken constant [11,35]: $\widetilde{u_i|\eta} = \widetilde{u}_i$. The conditionally filtered scalar dissipation rate is modelled with the Amplitude Mapping Closure (AMC) model [36]:

$$\widetilde{N|\eta} = \frac{\widetilde{N} G(\eta)}{\int_0^1 \widetilde{P}(\eta) G(\eta) d\eta} \tag{6}$$

This model requires an unconditional filtered scalar dissipation rate $\widetilde{N}$, which is found by summation of the resolved and the sub-grid scale contributions:

$$\widetilde{N} = \left(\frac{\nu}{Sc} + \frac{\nu_t}{Sc_t} \right) \frac{\partial \widetilde{\xi}}{\partial x_k} \frac{\partial \widetilde{\xi}}{\partial x_k} \tag{7}$$

In the AMC model as described, the conditional scalar dissipation rate profile as function of mixture fraction is prescribed by the bell-shape function, $G(\eta) = exp(-2[erf^{-1}(2\eta - 1)]^2)$.

In practical applications, a coarser grid is used to solve Eqs. (4) and (5) [11, 13]. Thus, the information must be induced from the LES mesh onto the CMC mesh. Here, volume averaging is applied to the unconditional quantities and the models for the conditional quantities are applied on the CMC resolution, in case of velocity and turbulent diffusivity, as in [12,13]. In case of scalar dissipation rate, PDF-weighted averaging is used and the AMC model is applied on the LES resolution. This is described in detail in [13].

The unconditional values are determined as:

$$\widetilde{Y}_\alpha = \int_0^1 \widetilde{Y_\alpha|\eta} \widetilde{P}(\eta) d\eta \tag{8}$$

$$\frac{1}{\bar{\rho}} = \int_0^1 \frac{1}{\overline{\rho|\eta}} \widetilde{P}(\eta) d\eta \tag{9}$$

The density-weighted filtered PDF ($\widetilde{P}(\eta)$) is assumed β-shaped and is calculated from the resolved mixture fraction and variance [13].

3 Chemistry mechanisms

Different detailed comprehensive chemistry mechanisms exist for H_2/O_2 reaction kinetics. In the present study, three chemistry mechanisms are applied to low-temperature (e.g. 900-1000K) auto-ignition in non-homogeneous mixtures. They differ by the reactions rate constants. In [21], we extensively discussed the chemistry behaviour for both cases [8,9].

Yetter et al. [24] presented a detailed mechanism (Table 1) containing 19 reversible reactions and 9 species (H_2, H, O, O_2, OH, H_2O, HO_2, H_2O_2, and N_2). This mechanism was further improved and adjusted to experimental data for a wider pressure range (0.3-15.7atm) and more narrow temperature range (850-1040K) by Mueller et al. [23], keeping 19 reactions as in [24]. This mechanism was extensively studied at flow reactor conditions, but it was not tested for other types of experiments. Subsequently, Li et al. [22] updated this H_2/O_2 mechanism, based upon new thermodynamic data and rate coefficients validated against a wider range of experimental conditions (298-3000K, 0.3-87atm). The following parameters were revised: the formation enthalpy of OH, the rate constant of the branching reaction (R1), the rate constant of (R8) and the low-pressure-limit rate constant of the competitive reaction (R9).

4 Test cases

4.1 Berkeley case

The Berkeley burner [8,10] consists of a fuel jet nozzle and a surrounding perforated disk. The jet nozzle inner diameter is 4.57mm (d) and the wall thickness is 0.89mm. The outer disk has a diameter of 210mm with an 87% blockage and consists of 2200 holes with a diameter of 1.58mm.

The fuel stream consists of hydrogen diluted with nitrogen, where the level of dilution is strongly different from the case [9] examined in the next section. The vitiated air consists of the products of a lean hydrogen/air flame. The stoichiometric mixture fraction is 0.474. The ratio between jet and co-flow velocity is higher than in the case of [9]. The low co-flow velocity suggests that turbulence is mainly created by shear stress. Table 2 summarizes the boundary conditions. The flame spontaneously ignited in the laboratory starting at downstream locations when the co-flow is operating and the jet flow is turned on. For these conditions, the observed lift-off height was about ten nozzle diameters [8]. There were no visually obvious auto-ignition events well below the lift-off height. A quantification of a most reactive mixture fraction was not reported.

As in [13], we use an in-house LES code, developed at Vrij Universiteit Brussel (VUB), Belgium [37] as flow field solver. In the CMC code, developed [38] and validated [12] at Cambridge University, equations (4) and (5) are solved, using the velocity and mixing field from the flow field solver. The mean density, required for the flow calculations, is obtained from the conditionally averaged values of the CMC calculations, weighted by the mixture fraction probability density function (β-PDF) (Eq. (9)). The computational domain extends axially $30d$ downstream from the jet inlet (roughly 137mm) and radially up to $20d$ (91.4mm). Results are obtained with the grid comprising $192 \times 48 \times 48$ cells in LES and $80 \times 4 \times 4$ cells in

CMC. The LES grid is stretched smoothly toward the co-flow in the radial direction and is expanded smoothly in the axial direction. The jet inlet is resolved with 12 × 12 cells in the inflow (x-z) plane. The CMC grid is expanded smoothly only in the axial direction. The mesh in mixture fraction space consists of 51 nodes, clustered around the most reactive mixture fraction ($\eta_{mr} = 0.0534$ for $T_{cf} = 1045$K). In [21], grid refinement was investigated and this resolution was shown to be sufficient. The most reactive mixture fraction has been determined with a stand-alone 0D-CMC code where the micro-mixing is switched off by using a scalar dissipation rate of $10^{-20}\mathrm{s}^{-1}$, giving thus a parallel solution to a series of homogeneous reactors of variable mixture fraction. In order to generate turbulence in the co-flow, the digital filter method [39] is used. The co-flow turbulence lengthscale was chosen to be 1.6mm, the size of the holes in the outer disk. The turbulence intensity is 5% [8,28]. The simulations are started from a developed inert flow field at time t_0. After 20ms, statistics are collected over a period of 17.5ms corresponding to 13.7 flow times, with one flow time being equal to axial length of the computational domain divided by the fuel exit velocity. Time averaged data are compared with the measurements. The lift-off height is defined as the location where OH mass fraction reaches 2×10^{-4} [27].

4.2 Cambridge case

The fuel, with mass fractions $Y(H_2) = 0.13$ and $Y(N_2) = 0.87$, is injected into a heated air co-flow through a 2.25mm (d) internal diameter pipe at ambient pressure. The configuration is confined with, the main test section consisted of 25.0mm (D) inner diameter vacuum insulated quartz tube. In the experiments, air velocities (u_{cf}) up to 35m/s, with air temperature (T_{cf}) up to 1015K, have been applied and the fuel velocity ranged from 20 to 120m/s, with fuel temperature (T_{fuel}) between 650K and 930K. For the given fuel composition, the stoichiometric mixture fraction, η_{st}, is 0.184. In [40] it is discussed how ignition always occurs at a well defined most reactive mixture fraction, η_{mr}. In the case under study, the most reactive mixture fraction (η_{mr}) is less than 0.041 [21], i.e. very lean. Consequently, the set-up is much more sensitive to perturbations in the co-flow than in the fuel jet. This is in detail examined in [21] and confirmed below.

Visual observation over a wide range of operating conditions showed the following qualitatively distinct regimes: 'no ignition', 'random spots', 'flashback' leading to anchored flames and 'lifted flame'. For low temperatures, no auto-ignition was observed within the length of the tube under investigation ('no ignition' regime). For a certain range of higher T_{cf} and/or Y_{H_2}, lower u_{cf} and/or u_{fuel}, instantaneous auto-ignition occurred in form of 'random spots'. In this statistically stationary regime, each auto-ignition event was associated with a short-lived ignition kernel. These ignition kernels were convected downstream by the flow before they disappeared. The ignition length increases by decreasing co-flow temperature or velocity. As the temperature was increased or dilution and velocities decreased, auto-ignition moved upstream towards the injector and became increasingly frequent. At even higher T_{cf}, Y_{H_2} and/or low u_{cf} as soon as the fuel was switched on, auto-ignition and subsequent flashback occurred. In this, 'flashback' regime, the first ignition kernel, randomly located in space, gave rise to a diffusion flame attached on the injector.

A CFD mesh of 192 × 48 × 48 cells is used, covering a domain of $30d$ (67.5mm) × 25mm (D) × 25mm (D). The CMC mesh consists of 80 × 8 × 8 cells. The number of nodes in mixture fraction space is 51 with clustering around η_{mr}. These resolutions have been shown to be sufficient in [13,21]. The inflow turbulence generator is based on the digital filter method [39], with chosen length and time scales of 4.5mm and 1ms, and turbulence intensity 12.5% [9]. At the air and fuel inlets, frozen inert mixing distributions in mixture fraction space are used.

For the present test case, [13] contains an extensive sensitivity study of the simulation results to mesh sizes, inflow (turbulence) conditions and numerical issues. The settings, mentioned above, have thus been verified in [13] and we do not repeat thus study here. Rather, we focus, here, on the case where T_{fuel} is 691K and T_{cf} is varied: 935K, 945K, 960K, 980K and 1009K. The fuel velocity, u_{fuel}, is first set to 120m/s while u_{cf} ranges from 20 to 35m/s. We in detail discuss instantaneous fields for 'random spots' regime what has not been done in previous study [13]. Comparing to [13], the sensitivity study is here extended to the influence of the fuel velocities as well as different chemistry mechanisms. Also, the feasibility of using first order CMC for the test case at hand is discussed by looking at scalar dissipation profiles.

In the literature, several definitions exist to determine ignition. We use the criterion of [27], where auto-ignition is defined as the first point where $Y(OH)$ exceeds $2{\times}10^{-4}$. In [13,21], we showed that this leads to almost identical results as the criterion of [16], based on a maximum local temperature increase of 1% over the nominal co-flow temperature, for the test case at hand.

5 Results and Discussion

5.1 Berkeley case

The radial profiles of mean mixture fraction at various axial locations (y/d = 1, 8, 10, 11, 14, 26) in the lifted flame are shown in Fig. 1 for the conditions listed in Table 2. In the experiment, the mixture fraction is defined based on [41], modified for H_2/N_2 system. Good agreement of measured and computed mixture fraction fields is observed for most axial positions, despite some overprediction from at y/d = 14 onwards. Good agreement, particularly in the jet stream and the layer between jet and co-flow stream, shows that the grid choice with the refinement in the jet region is satisfactory to reproduce the mixing sufficiently accurately for this problem. The good quality of mixture fraction profiles is very important for the quality of the values for all species.

Fig. 2 shows the lift-off heights (H) for a range of a co-flow temperatures (T_{cf} = 1010K, 1022K, 1030K, 1045K, 1060K and 1080K) using the chemistry mechanism of Li et al. [22]. In Fig. 2, the simulation results are compared with the data measured independently by Cabra et al. [8], Gordon et al. [10] and Wu et al. [42]. The Gordon et al. results (a) and (b) refer to measurements taken in two separate experiments. The flame with T_{cf} = 1080K is an attached flame in the simulations. When the temperature is reduced, a lifted flame is observed. The results confirm previous findings with transported PDF simulations [27] which showed that the flame is extremely sensitive to changes in the co-flow temperature. In their cal-

culations a lift-off height of $H/d = 10$ corresponded to a co-flow temperature of 1033K.

The uncertainty in the temperature measurements reported in [8] was of the order of 30K. This is indicated by the horizontal error bar in Fig. 2. It is clear that the lift-off height predictions are within the experimental uncertainty and in good agreement with the measurements of [42]. The good quality of this results allows the study of the Cambridge case.

5.2 Cambridge case

5.2.1 Global discussion

Figures 3 and 4 show radially and time averaged conditional temperature and species mass fractions (OH, H_2O, H, HO_2) profiles, as obtained on the CMC mesh. The results are presented for $T_{cf} = 960$K, $u_{cf} = 26$m/s and the mechanism of [22]. Each line in Fig. 3 corresponds to one plane of CMC cells. Fig. 4 is a 2D representation of Fig. 3 for three axial locations. Time averaging for the LES and CMC results was performed with data collected over 10ms, approximately $18L/u_{fuel}$ ($L = 67.5$mm), after a statistically steady state has been reached. A lifted flame is recognized. The lift-off height, defined using the criterion of [27], is approximately 11.2mm ($5d$). Fig. 3 illustrates the gradual evolution of flame structure from the inert ('frozen') distribution at the inlet to fully 'burning' distributions. The maximum temperature (2400K), H_2O (0.195) and OH mass fraction (0.0136) are reached near stoichiometry. The region of high OH/H_2O concentration corresponds to the high temperature region. The highest values of H are found at the rich side. The highest concentrations of HO_2 radical are found in the region between stoichiometric and most reactive mixture fraction isolines, at the flame base. The observations in Figs. 3 and 4 indicate auto-ignition taking place.

Auto-ignition is indeed characterized by a build-up of concentration of HO_2 prior to ignition, while premixed flame propagation is characterized by simultaneous initiation of build up of all radicals [10]. Just upstream of the auto-ignition point there is build up of HO_2 radical, ahead of the flame edge (Fig. 3), prior to creation H_2O, H and OH, indicating that the flame is stabilized by auto-ignition at its base. Note the travelling of the peak of HO_2 from the most reactive mixture fraction towards $\eta = 0$ and $\eta = 1$ after auto-ignition. These reaction fronts consume the already premixed fuel-air and result in the establishment of a normal non-premixed flame. As Fig. 3 shows, this condition is not fully achieved for all mixture fractions, at the very rich side, at the end of the simulation domain. However, such rich mixture fractions do not appear in physical space in that region. The non-premixed flame condition is met from $y = 0.018$m onwards, i.e. from $y = 1.6 \times L_{ign}$ onwards.

Fig. 5 shows radially and time averaged conditional scalar dissipation rate. PDF averaging causes a deviation from the bell-shaped profile, inherent to the AMC model, particularly at the inlet. The conditional scalar dissipation rate is high in the pre-ignition region and rapidly decays further downstream. Fig. 6 shows the evolution of the maximum values of conditional temperature and conditional scalar dissipation rate in the axial direction, as well as conditional scalar dissipation rate around η_{mr}. At the flame base, the conditional scalar dissipation rate is already

relatively low, compared to the values at the inlet. As a consequence, at the flame base, the chemical reaction source term (T_3) is balanced by convection (T_1) and, to minor extent, by scalar dissipation rate (T_2), while diffusion (T_4) is negligible [13]. Following [10], this is considered a second indicator of flame stabilization by auto-ignition, where indeed, a balance is expected between reaction and convection, with no contribution from diffusion. In contrast, propagating premixed flames are characterized by a reaction zone where the dominant balance is between reaction and diffusion, convection playing a minor role.

The rapid decay of the conditional scalar dissipation rate and the fact that the scalar dissipation rate is low (around $5s^{-1}$), particularly at η_{mr}, for a significant period (or distance in physical space) before auto-ignition takes place (Figs. 5 and 6), explains why first-order CMC, which is in general expected to be less accurate than second-order CMC, is adequate for the problem at hand. In [38], it was shown for n-heptane auto-ignition and the present configuration that second-order closure is important only when the mean scalar dissipation rate is high and conditional fluctuations are large. In the case under study the region of high scalar dissipation rate is not close to the region where auto-ignition occurs, so that second-order effects are less important.

5.2.2 Sensitivity to velocities and temperature

The inlet fluctuations, the co-flow temperature and the co-flow velocity affect the first emergence of auto-ignition. The influence of the inlet fluctuations is examined in [13]. Here, focus is on the detail sensitivity of the system to the co-flow temperature, where range of co-flow temperatures: 935K, 945K, 960K, 980K and 1009K (Fig. 7) is used as well as different chemistry mechanisms. Fig. 7 shows contours of the time averaged temperature and OH mass fraction in a symmetry plane for mechanism of [22]. The auto-ignition location, which can be identified as a sudden increase in the average OH mass fraction above a certain threshold value ($Y(OH) = 2\times10^{-4}$), shifts closer to the nozzle as the co-flow temperature increases, as expected. The similarity of temperature and OH fields confirms previous findings [21] that both temperature and OH mass fraction can be used for the determination of the ignition length.

At the lowest co-flow temperatures ($T_{cf} = 935$K), the 'random spots' regime is obtained, one of the most challenging regimes to simulate. It is described as random recurring auto-ignition events. The auto-ignition kernels, generated at a certain distance from the nozzle, are convected out of the domain. At this temperature, the apparent average 'flame' stabilizes further downstream, but also the maximum temperature in physical space is not encountered around stoichiometry, but in the lean region (Fig. 7). Clearly, such behaviour does not correspond to a lifted flame.

In Fig. 8, a time sequence of OH mass fraction in a symmetry plane for $T_{cf} =$ 935K and mechanism of Li et al. [22] is shown to illustrate this. The time difference between two snapshots is 0.03ms. At time t_1, an auto-ignition kernel, pointed with the arrow, is present. At times t_2 and t_3, the kernel is convected downstream. Further in time, t_4, the kernel starts to disappear while being convected downstream. At t_5, while the OH concentration of the original kernel is still decreasing, a new kernel appears (second arrow). The new kernel is formed at roughly the same downstream location as the original one. Similar observations were made in [43]. This is followed by the growth of the new kernel and further disappearing

of the old one (t_6, t_7 and t_8). No ignition is observed below the height where the reaction stabilises. The process is highly transient but statistically stationary. Qualitatively, this regime is similar to the 'random spots' observed experimentally. 'No ignition' regime is not shown, but it is obtained for co-flow temperatures lower than 930K.

At higher co-flow temperatures, kernels are formed more frequently , in qualitative agreement with experimental data [44] (although the reported data on the autoignition spot frequency were given for acetylene as fuel, the trend of auto-ignition spot frequency with flow speed and air temperature are expected to carry over to the hydrogen case). Also, with high co-flow temperature, the kernels are convected downstream forming a diffusion flame (T_{cf} =945K, Fig. 7). Further increase in temperature results in flame stabilised closer to the injector, in the region of high local scalar dissipation rate. In these cases, the chemical reaction rates are enhanced by the increase of temperature and hence auto-ignition occurs closer to the injector. At temperatures, 960K and 980K, auto-ignition first occurs downstream of a final stabilisation location, and subsequently, the flame seems to move upstream by spontaneous ignition. At these temperatures, the convection-reaction balance is observed, the diffusion being small, as described in [13]. As mentioned above, this means that the flames at these higher co-flow temperatures are lifted flames stabilised by auto-ignition. At these temperatures, a higher co-flow velocity is needed to access the random spots regime. For even higher co-flow temperatures the 'flashback' regime is recovered: as soon as the fuel mixture is injected, auto-ignition and 'flashback' occur, resulting in a jet diffusion flame stabilised on the injector nozzle [9]. This is observed for co-flow temperature 1009K (Fig. 7).

In other words, Figures 7 and 8 illustrate that the global experimental observations are well captured: the four regimes observed experimentally [9], are recovered, which is a key result and which is in line with results reported in [20].

In Fig. 9, the ignition length observed in experiments (L_{min}), is compared to the present simulation results. The sensitivity of the results to the chemistry mechanism is discussed below, but clearly (L_{min}) reduces with increasing T_{cf}, as it should. Notably, for the simulation results to be within the same range as the experimental data, the latter must be shifted by 50K. This is in line with results reported in e.g. [16, 20]. Indeed, in [16], although a figure is presented similar to Fig. 9, showing L_{ign} as function of T_{cf} (albeit for u_{fuel} = 26m/s instead of 120m/s), it is stated that for T_{cf} =960K flashback is obtained where flame attaches at the nozzle. In other words, in [16] the point of first ignition is presented, not the steady situation. In contrast hereto, Fig. 9 reports the steady state situation, i.e. L_{ign} would have been shown as 0 for an attached flame, rather than $15d$ (as done in [16]). In [20], flashback is reported for T_{cf} =980K, whereas the experimental data clearly report a lifted flame far away from the nozzle, which again confirms that L_{ign} is under-predicted for a certain value of T_{cf}.

The evolution of L_{ign} with T_{cf} in the simulation results is clearly non-linear, whereas the experimental data as presented may give the impression that the dependence is more or less linear. This, however, is a consequence of the fact that the data only cover a relatively limited range of conditions. Indeed, in [45], from the group where the experiments took place, it is explicitly confirmed that the dependence is non-linear.

As expected, the effect of the fuel velocity is negligible (Fig. 10). This is not surprising since the auto-ignition, for the case under study, occurs at very lean side.

The effect of the co-flow velocity has been investigated for T_{cf} = 945K and 960K, with u_{cf} = 20, 26 and 35m/s (Fig. 11). At higher co-flow velocity, the convection term T_1 (Eqs. 4 and 5) becomes dominant what causes the flame stabilization further downstream. This confirms the important impact of the convection on the position of the stabilization point for the test case at hand [13]. The experimental finding that L_{min} increases with u_{cf} is well captured. The flame sensitivity to the change in u_{cf} for T_{cf} = 945K is stronger than for T_{cf} = 960K, an increase from 20m/s to 35m/s moves the flame for 10.9mm further downstream with T_{cf} = 945K, while with T_{cf} = 960K the shift is approximately 5.4mm. However, the experimental finding that an estimated residence time until ignition also increases with u_{cf} seems not to be captured well. This residence time scales with L_{min}/u_{cf}; the different velocity in the jet and co-flow have to be taken into account for more exact estimates. This discrepancy may be due to scalar dissipation model used in the present LES-CMC implementation. Note that RANS-CMC of n-heptane in the same geometry [46] has captured this trend after an effort to predict correctly the mean scalar dissipation (in inert flow), which gives credence to attributing the present discrepancy to the LES scalar dissipation rate model. Such a study is considered beyond the scope of the present paper.

The results in Fig. 11, also indicate that the flame is basically chemically controlled, with convection determining the location of auto-ignition and flame stabilization. In [13], the stabilization mechanism is explored, auto-ignition or premixed flame propagation, by quantifying the balance of the terms in the CMC equation. No evidence of premixed flame propagation is found: the diffusion in physical space was negligible.

5.2.3 Sensitivity to the chemistry mechanism

As shown above, the flame is stabilized by auto-ignition and therefore sensitive to chemical kinetics. The influence of the choice of chemical kinetics is investigated for three mechanisms [22–24]. Fig. 9 shows that all mechanisms capture the sensitivity to the temperature changes similarly, while the absolute values are somewhat different for each mechanism. After ignition, all mechanisms also perform in a similar way (Fig. 12, to be compared with Fig. 3). The mechanism of [24] predicts the highest lift-off heights while mechanism of [22] the shortest. The mechanism of [24] also exhibits stronger sensitivity to the co-flow temperature than the other two (Fig. 9). For T_{cf} = 935K, no ignition was even observed with mechanism [24]. Differences between mechanisms become smaller with increasing co-flow temperature, in agreement with [27] (for the test case of [8] and mechanisms of [22, 23]). The results are also in good agreement with [21].

In [28, 29], a RANS-based PDF method was applied and it was reported that the predicted ignition delay times were very sensitive to the chemical kinetic rates (for the case of [8]). In [21] we illustrate that the sensitivity for the test case at hand [9] is not the same as for case of [8], particularly due to differences in fuel composition, although the main trends are quite similar. This justifies our sensitivity study for [9].

The sensitivity to the co-flow velocity was also performed for $T_{cf} = 960$K and different chemistry mechanisms (Fig. 13). With increasing co-flow velocity, all mechanisms behave in a similar way: the lift-off height increases and the shift is proportional to the lift-off height for $u_{cf} = 26$m/s. This was as well, not reported before.

6 Conclusions

The conditional moment closure with detailed chemistry has been applied, in combination with LES, to a nitrogen-diluted hydrogen jet in a turbulent co-flow stream of preheated air. The results are qualitatively consistent with experimental data. Flame stabilization occurs closer to the nozzle with a decrease in co-flow velocity and for an increase in co-flow temperature. An increase in temperature enhances the chemical reaction and hence auto-ignition occurs closer to the injector. With the present approach, all observed auto-ignition regimes in this burner have been recovered. In contrast to what was reported in our previous study [13], the random spots regime has been discussed.

The effect of the co-flow velocity is important since auto-ignition occurs at the lean side. With higher co-flow velocity, the influence of convection becomes stronger and the flame stabilizes further downstream. The effect of the fuel velocity on the other hand is negligible.

The choice of the chemistry mechanism is important, particularly for lower co-flow temperatures. Different chemistry mechanisms have been tested and have been shown to exhibit a similar qualitative behaviour. Different boundary conditions are required in order to yield the same ignition length. With increasing co-flow temperature, the differences in ignition length diminish. The good agreement with [21] has not been reported before.

Compared to [13], first order CMC has also been illustrated to be a good modelling choice for the test cases at hand by looking at the scalar dissipation rate profiles.

References

1. Mastorakos, E.: Ignition of turbulent non-premixed flames. Prog. Energy Combust. Sci. **35**, 57–97 (2009)
2. Klimenko, A.Y., Bilger, R.W.: Conditional moment closure for turbulent combustion. Prog. Energy Combust. Sci. **25**, 595–687 (1999)
3. Pope, S.B.: PDF methods for turbulent reactive flows. Prog. Energy Combust Sci **11**, 119–192 (1985)
4. Di Mare, F., Jones, W.P., Menzies, K.R.: Large eddy simulation of a model gas turbine combustor. Combust. Flame **137**, 278–294 (2004)
5. Pitsch, H., Steiner, H.: Large-eddy simulation of a turbulent piloted methane/air diffusion flame (Sandia flame D). Phys. Fluids **12**, 2541–2554 (2000)
6. Ihme, M., See, C.S.: Prediction of auto-ignition in a lifted methane/air flames using an unsteady flamelet/progress variable model. Combust. Flame **157**, 1850–1862 (2010)
7. Ramaekers, W.J.S., van Oijen, J.A., de Goey, L.P.H.: A priori testing of flamelet generated manifolds for turbulent partially premixed methane/air flames. Flow Turbl. Combust. **84**, 439–458 (2010)
8. Cabra, R., Myhrvold, T., Chen, J.Y., Dibble, R.W., Karpetis, A.N., Barlow, R.S.: Simultaneous laser Raman-Rayleigh-Lif measurements and numerical modeling results of a lifted turbulent H_2/N_2 jet flame in a vitiated coflow. Proc. Combust. Inst. **29**, 1881–1888 (2002)

9. Markides, C.N., Mastorakos, E.: An experimental study of hydrogen auto-ignition in a turbulent co-flow of heated air. Proc. Combust. Inst. **30**, 883–891 (2005)
10. Gordon, R.L., Masri, A.R., Pope, S.B., Goldin, G.M.: A numerical study of auto-ignition in turbulent lifted flames issuing into vitiated co-flow. Combust. Theory Model. **11**, 351–376 (2007)
11. Triantafyllidis, A., Mastorakos, E.: Implementation issues of the conditional moment closure model in large eddy simulations. Flow Turbul. Combust. **84**, 481–512 (2010)
12. Triantafyllidis, A., Mastorakos, E., Eggels, R.L.G.M.: Large eddy simulations of forced ignition of a non-premixed bluff-body methane flame with conditional moment closure. Combust. Flame **156**, 2328–2345 (2009)
13. Stanković, I., Triantafyllidis, A., Mastorakos, E., Lacor, C., Merci, B.: Simulation of hydrogen auto-ignition in a turbulent co-flow of heated air with LES and CMC approach. Flow Turb. Combust. **86**, 689–710 (2011)
14. Gordon, R.L., Masri, A.R., Mastorakos, E.: Heat release rate as represented by [OH]x[CH_2O] and its role in autoignition. Combust. Theory Model. **13**, 645–670 (2009)
15. Gordon, R.L., Masri, A.R., Mastorakos, E.: Simultaneous Rayleigh temperature, OH- and CH_2O-LIF imaging of methane jets in a vitiated coflow. Combust. Flame **155**, 181–195 (2008)
16. Jones, W.P., Navarro-Martinez, S.: Study of hydrogen auto-ignition in a turbulent air co-flow using a large eddy simulation approach. Comput. Fluids **37**, 802–808 (2008)
17. Jones, W.P., Navarro-Martinez, S., Rohl, O.: Large eddy simulation of hydrogen auto-ignition with a probability density function method. Proc. Combust. Inst. **31**, 1765–1771 (2007)
18. Galpin, J., Angelberger, C., Naudin, A., Vervisch, L.: Large-eddy simulation of H_2-air auto-ignition using tabulated detailed chemistry. J. Turbul. **9**, 1–21 (2008)
19. Patwardhan, S.S., Lakshmisha, K.N.: Auto-ignition of turbulent hydrogen jet in a co-flow of heated air. Int. J. Hydrogen Energy **33**, 7265–7273 (2008)
20. Navarro-Martinez, S., Kronenburg, A.: Flame stabilization mechanisms in lifted flames. Flow Turbl. Combust. **87**, 377–406 (2011)
21. Stanković, I., Merci, B.: Analysis of auto-ignition of heated hydrogen/air mixtures with different detailed reaction mechanisms. Combust. Theory Model. **15**, 409–436 (2011)
22. Li, J., Zhao, Z., Kazakov, A., Dryer, F.L.: An updated comprehensive kinetic model of hydrogen combustion. Inter. J. Chem. Kinet. **36**, 566–575 (2004)
23. Mueller, M.A., Kim, T.J., Yetter, R.A., Dryer, F.L.: Flow reactor studies and kinetic modeling of the H_2/O_2 reaction. Inter. J. Chem. Kinet. **31**, 113–125 (1999)
24. Yetter, R.A., Dryer, F.L., Rabitz, H.: A comprehensive reaction-mechanism for carbon-monoxide hydrogen oxygen kinetics. Combust. Sci. Technol. **79**, 97–128 (1991)
25. O'Conaire, M., Curran, H.J., Simmie, J.M., Pitz, W.J., Westbrook, C.K.: A comprehensive modeling study of hydrogen oxidation. Inter. J. Chem. Kinet. **36**, 603–622 (2004)
26. Konnov, A.A.: Remaining uncertainties in the kinetic mechanism of hydrogen combustion. Combust. Flame **152**, 507–528 (2008)
27. Cao, R.R., Pope, S.B., Masri, A.R.: Turbulent lifted flames in a vitiated co-flow investigated using joint PDF calculations. Combust. Flame **142**, 438–453 (2005)
28. Masri, A.R., Cao, R., Pope, S.B., Goldin, G.M.: PDF calculations of turbulent lifted flames of H_2/N_2 fuel issuing into a vitiated co-flow. Combust. Theory Model. **8**, 1–22 (2004)
29. Gkagkas, K., Lindstedt, R.P.: The impact of reduced chemistry on auto-ignition of H_2 in turbulent flows. Combust. Theory Model. **13**, 607–643 (2009)
30. Pope, S.B.: Turbulent Flows. Cambridge University Press, Cambridge (2000)
31. Smagorinsky, J.: General circulation experiments with the primitive equations. Mon. Weather Rev. **91**, 99–164 (1963)
32. Pierce, C.D., Moin, P.: A dynamic model for subgrid-scale variance and dissipation rate of a conserved scalar. Phys. Fluids **10**, 3041–3044 (1998)
33. Girimaji, S.S., Zhou, Y.: Analysis and modeling of subgrid scalar mixing using numerical data. Phys. Fluids **8**, 1224–1236 (1996)
34. Navarro-Martinez, S., Kronenburg, A., Di Mare, F.: Conditional moment closure for large eddy simulations. Flow Turbul. Combust. **75**, 245–274 (2005)
35. Kim, S.H., Pitsch, H.: Mixing characteristics and structure of a turbulent jet diffusion flame stabilized on a bluff-body. Phys. Fluids **18**, 075103 (2006)
36. O'Brien, E.E., Jiang, T.L.: The conditional dissipation rate of an initially binary scalar in homogeneous turbulence. Phys. Fluids **3**, 3121–3123 (1991)

37. Broeckhoven, T.: LES of turbulent combustion: numerical study and applications. PhD thesis, VUB - Department of Mechanical engineering (2007)
38. De Paola, G., Kim, I.S., Mastorakos, E.: Second-order conditional moment closure simulations of autoignition of an n-heptane plume in a turbulent co-flow of heated air. Flow Turbl. Combust. **82**, 455-475 (2009)
39. Klein, M., Sadiki, A., Janicka, J.: A digital filter based generation of inflow data for spatially developing direct numerical or large eddy simulations. J. Comput. Phys. **186**, 652–665 (2003)
40. Mastorakos, E., Baritaud, T.A., Poinsot, T.J.: Numerical simulations of auto-ignition in turbulent mixing flows. Combust. Flame **109**, 198–233 (1997)
41. Bilger, R.W., Starner, S.H., Kee, R.J.: On reduced mechanisms for methane-air combustion in nonpremixed flames. Combust. Flame **80**, 135–149 (1990)
42. Wu, Z., Starner, S.H., Bilger, R.W.: Lift-off heights of turbulent H_2/N_2 jet flames in a vitiated co-flow. Proceedings of the 2003 Australian Symposium on Combustion and the Eighth Australian Flame Days,The Combustion Institute (2003)
43. Jones, W.P., Navarro-Martinez, S.: Numerical study of n-heptane auto-ignition using LES-PDF methods. Flow Turbl. Combust. **83**, 407–423 (2009)
44. Markides, C.N., Mastorakos, E.: Experimental investigation of the effects of turbulence and mixing on autoignition chemistry. Flow Turbl. Combust. **86**, 585-608 (2011)
45. Lee, C. W. and Mastorakos, E.: Transported scalar PDF calculations of autoignition of a hydrogen jet in a heated turbulent co-flow. Combust. Theory Model. **12**, 1153-1178 (2008)
46. Markides, C.N., De Paola, G., Mastorakos, E.: Measurements and simulations of mixing and auto-ignition of an n-heptane plume in a turbulent flow of heated air. Exp. Therm. Fluid Sci. **31**, 393-401 (2007)

Table 1: H_2/O_2 reaction mechanism [24].

R1	$H + O_2 = O + OH$
R2	$O + H_2 = H + OH$
R3	$OH + H_2 = H + H_2O$
R4	$OH + OH = O + H_2O$
R5	$H_2 + M = H + H + M$
R6	$O + O + M = O_2 + M$
R7	$O + H + M = OH + M$
R8	$H + OH + M = H_2O + M$
R9	$H + O_2 + M = HO_2 + M$
R10	$HO_2 + H = H_2 + O_2$
R11	$HO_2 + H = OH + OH$
R12	$HO_2 + O = OH + O_2$
R13	$HO_2 + OH = H_2O + O_2$
R14	$HO_2 + HO_2 = H_2O_2 + O_2$
R15	$H_2O_2 + M = OH + OH + M$
R16	$H_2O_2 + H = H_2O + OH$
R17	$H_2O_2 + H = H_2 + HO_2$
R18	$H_2O_2 + O = OH + HO_2$
R19	$H_2O_2 + OH = H_2O + HO_2$

Table 2: Boundary conditions [8, 27].

Item	Co-flow	Fuel jet
Diameter [mm]	210	4.57
Velocity [m/s]	3.5	107
Temperature [K]	1045	305
$X(H_2)$ [-]	0.0005	0.2537
$X(O_2)$[-]	0.1474	0.0021
$X(N_2)$ [-]	0.7534	0.7427
$X(H_2O)$ [-]	0.0989	0.0015

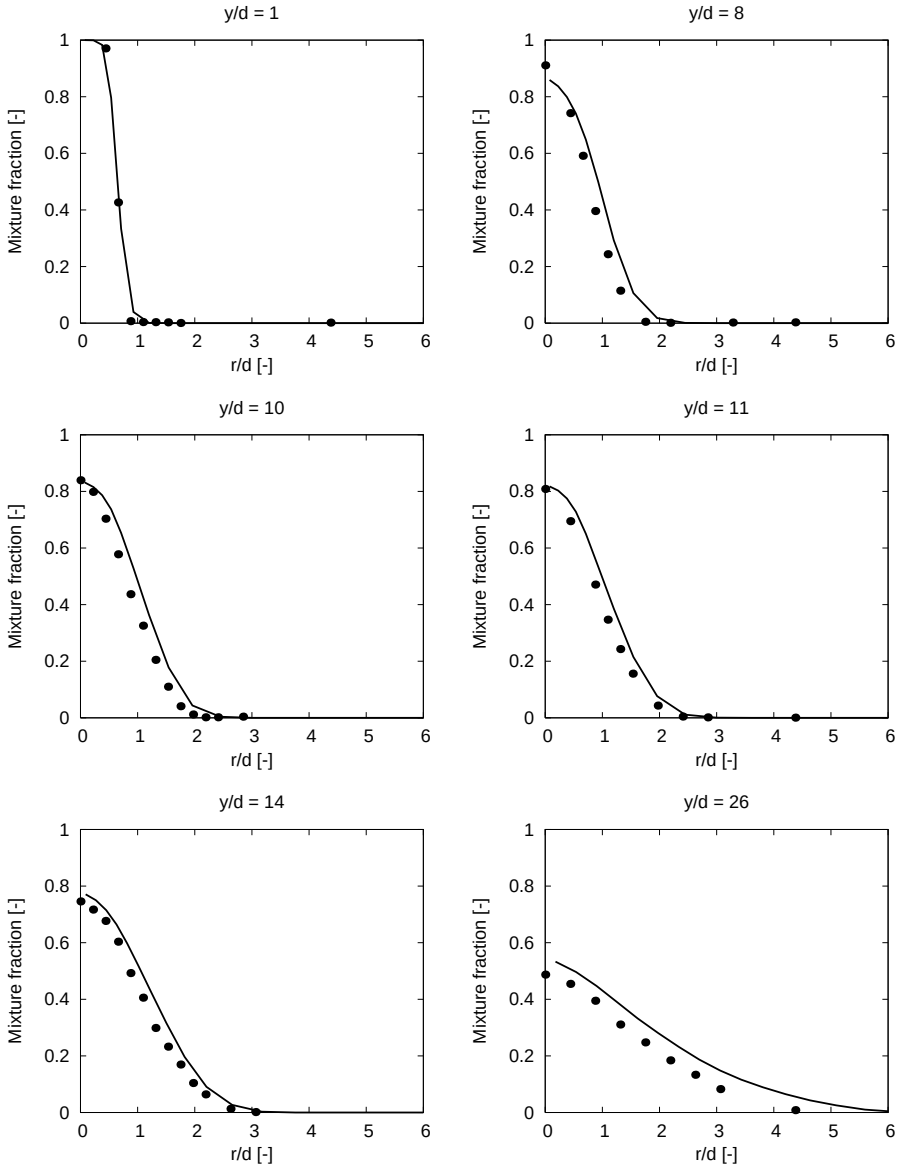

Fig. 1: Radial profiles of mixture fraction at six axial stations ($T_{cf} = 1045$K and mechanism of [22]). Filled circles: experiments [8]. Lines: present results.

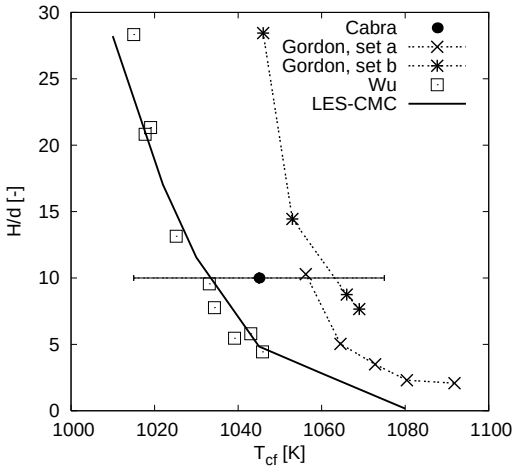

Fig. 2: Lift-off height as a function of the co-flow temperature (mechanism of [22]).

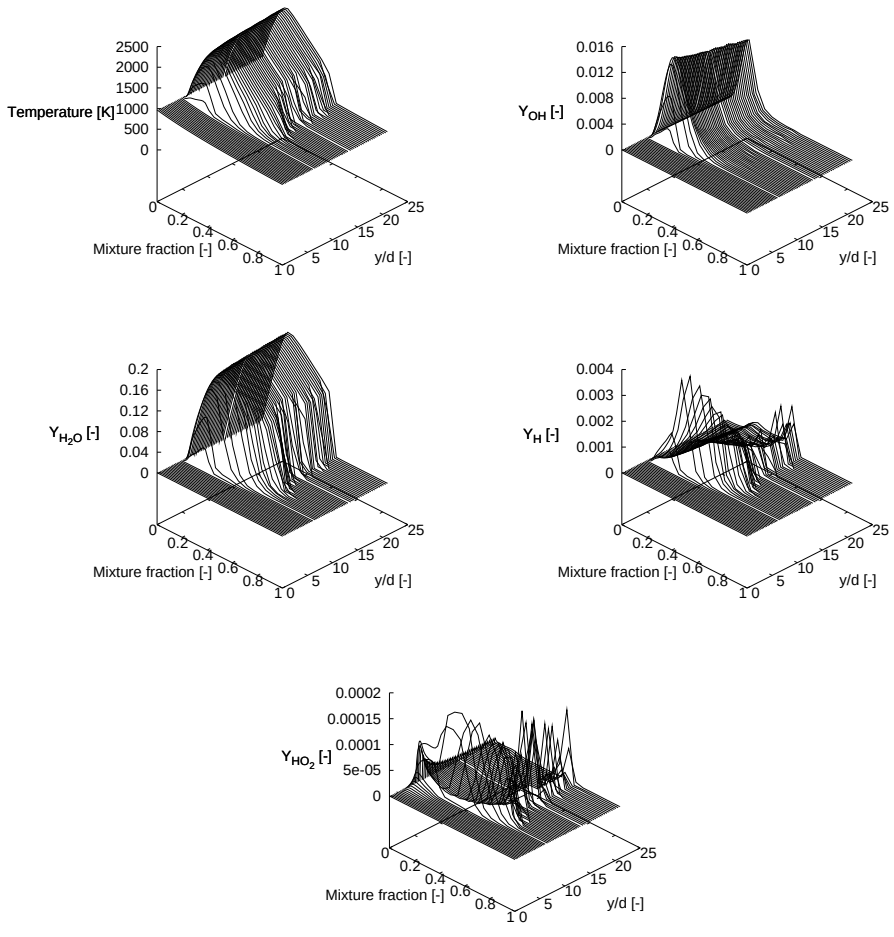

Fig. 3: Evolution in the axial direction of conditional temperature and species mass fractions (time and cross-stream averaged) as function of mixture fraction ($T_{cf} = 960K$, $u_{cf} = 26$m/s and mechanism of [22]).

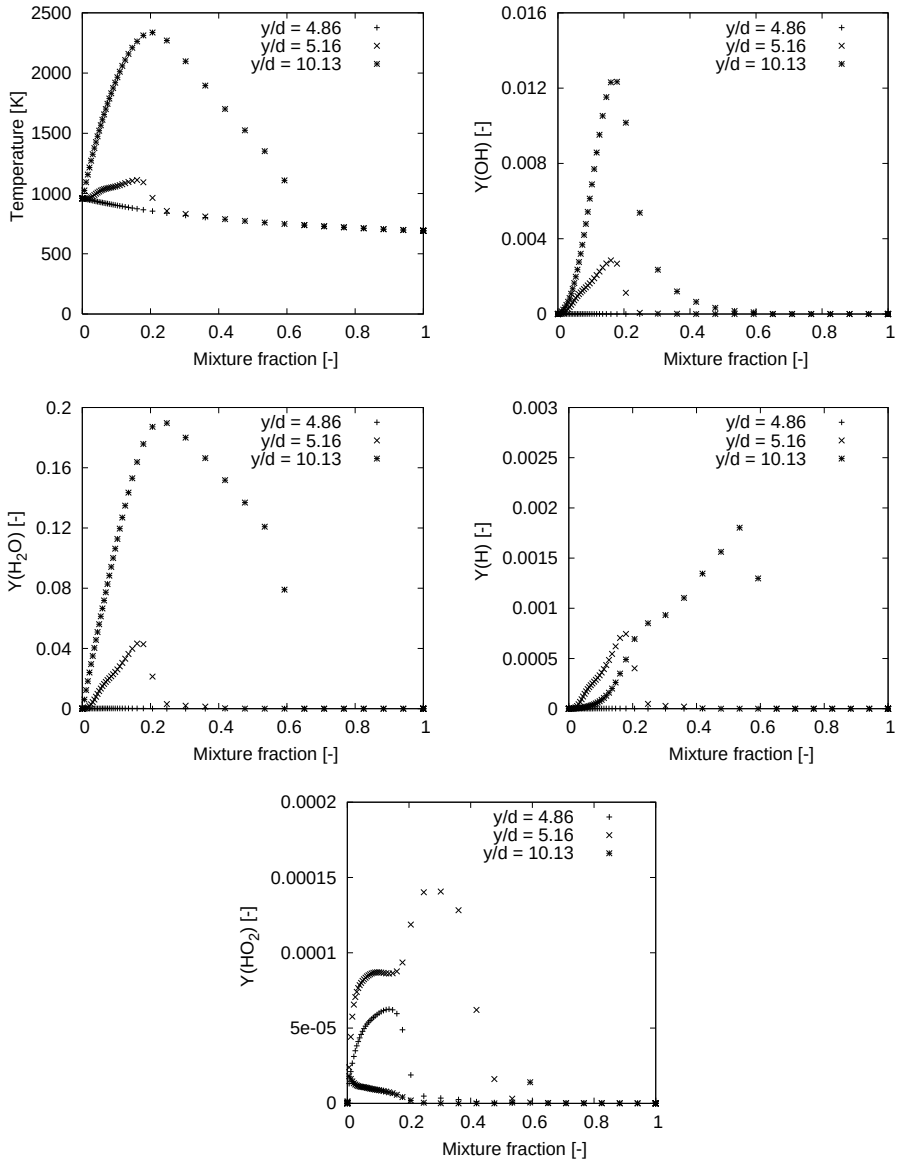

Fig. 4: Conditional temperature and species mass fractions as function of mixture fraction for three different axial locations ($T_{cf} = 960K$, $u_{cf} = 26$m/s and mechanism of [22]).

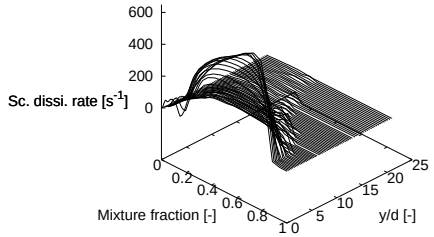

Fig. 5: Evolution in the axial direction of conditional scalar dissipation rate (time averaged and cross-stream averaged) as function of mixture fraction ($T_{cf} = 960K$, $u_{cf} = 26$m/s and mechanism of [22]).

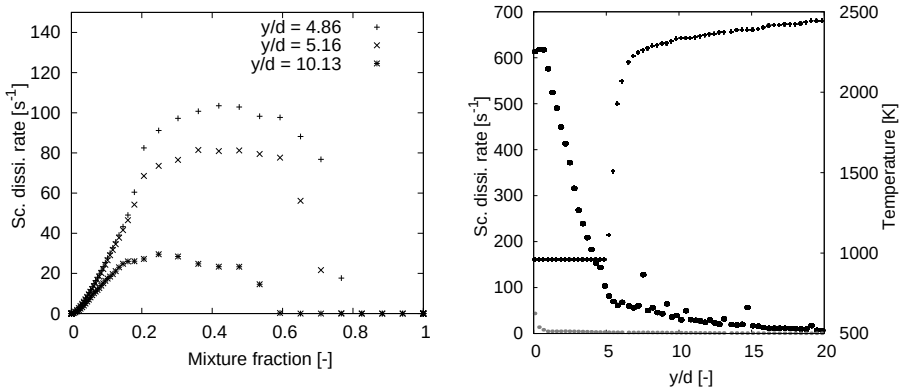

Fig. 6: Left: Conditional scalar dissipation rate as function of mixture fraction for three different axial locations ($T_{cf} = 960K$, $u_{cf} = 26$m/s and mechanism of [22]). Right: Maximal conditional temperature (crosses), maximal conditional scalar dissipation rate (black circles) and conditional scalar dissipation rate around η_{mr} (grey circles).

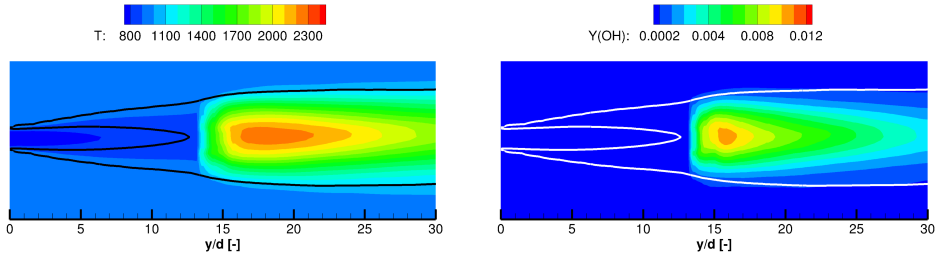

(a) $T_{cf} = 935$K

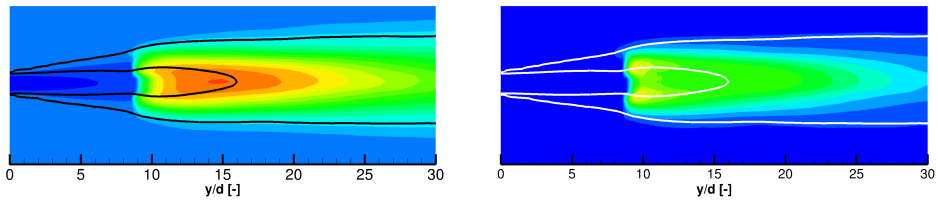

(b) $T_{cf} = 945$K

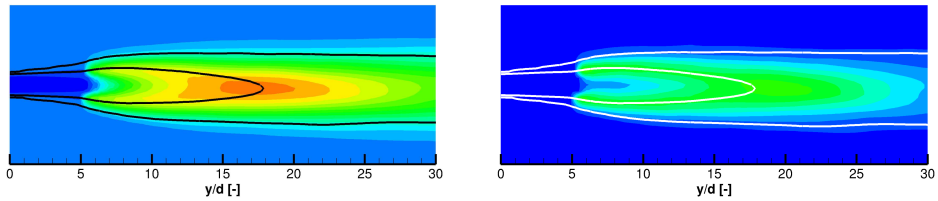

(c) $T_{cf} = 960$K

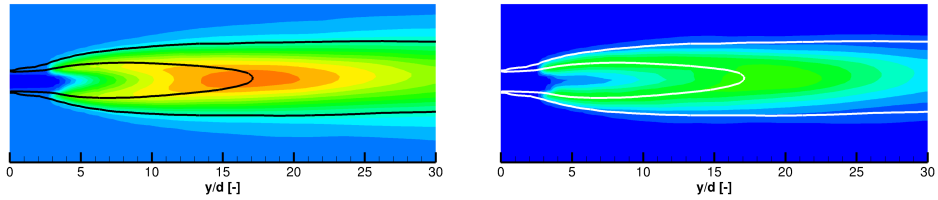

(d) $T_{cf} = 980$K

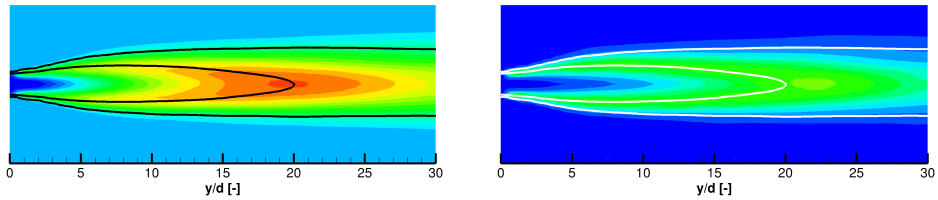

(e) $T_{cf} = 1009$K

Fig. 7: Contours of the time averaged temperature and OH mass fraction in a symmetry plane with different co-flow temperatures (mechanism of [22]). Inner isoline: η_{st}. Outer isoline: η_{mr}.

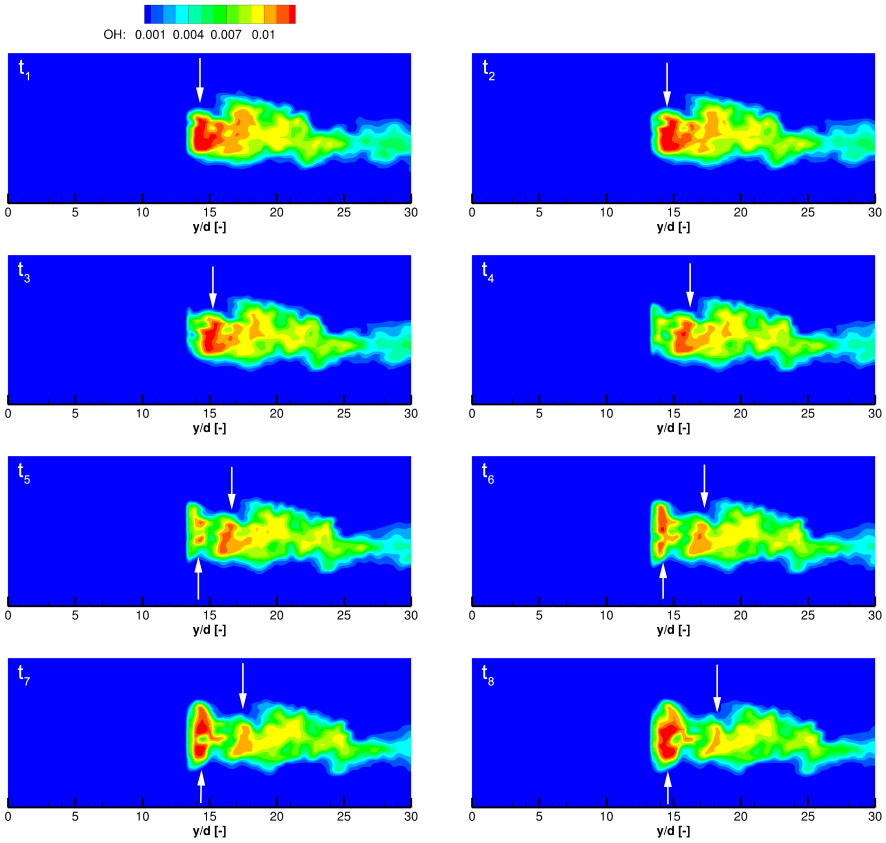

Fig. 8: Time sequence of OH mass fraction in a symmetry plane for the random spots regime (T_{cf} = 935K and mechanism of [22]). Time interval between frames: 0.03ms.

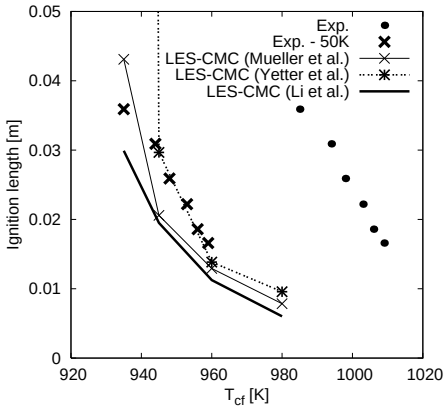

Fig. 9: Influence of co-flow temperature for u_{cf} = 26 m/s on the flame lift-off height. The LES-CMC results are at the statistically steady state.

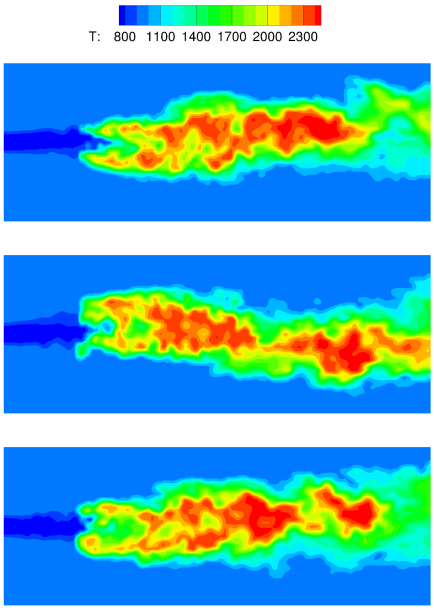

Fig. 10: Influence of fuel velocity on the flame lift-off height (u_{cf} = 26 m/s, T_{cf} = 960K and mechanism of [22])). Top: u_{fuel} = 110 m/s. Middle: u_{fuel} = 120 m/s. Bottom: u_{fuel} = 130 m/s.

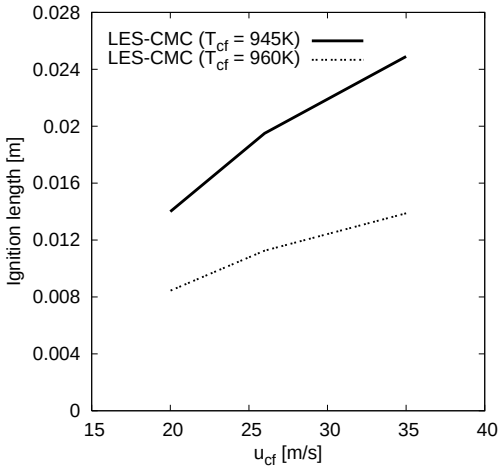

Fig. 11: Influence of co-flow velocity on the flame lift-off height (mechanism of [22])).

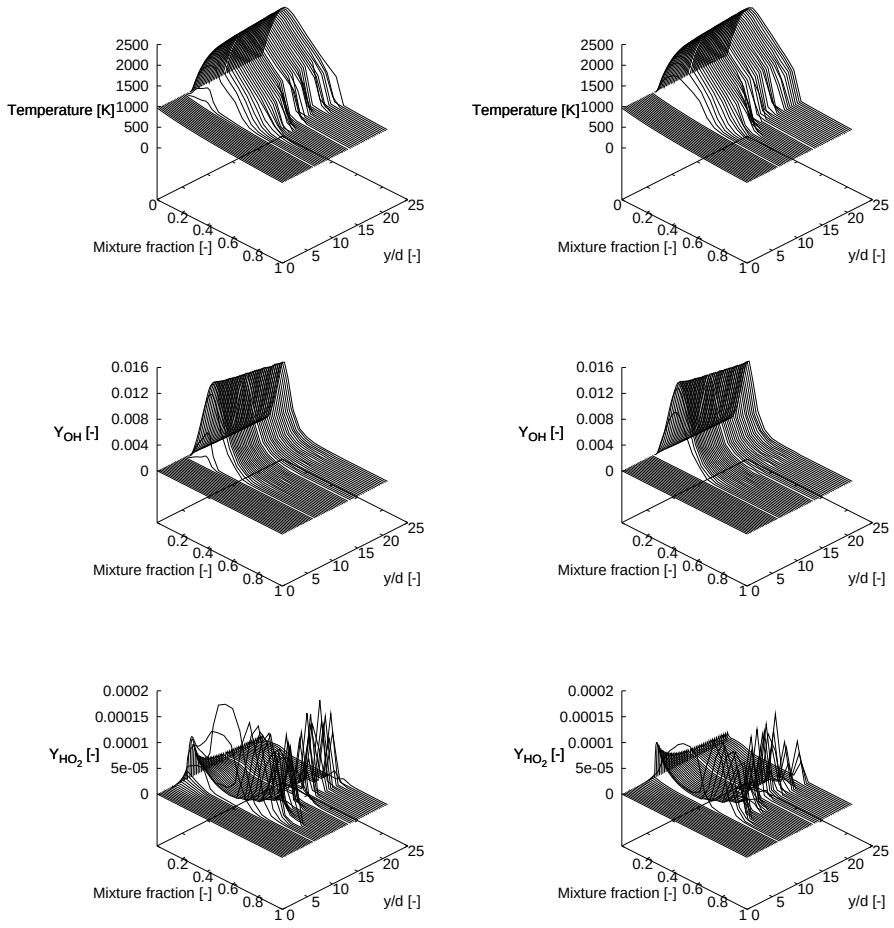

Fig. 12: Evolution in the axial direction of conditional temperature and species mass fractions (time and cross-stream averaged) as function of mixture fraction ($T_{cf} = 960$K, $u_{cf} = 26$m/s). Right: mechanism of [23]. Left: mechanism of [24].

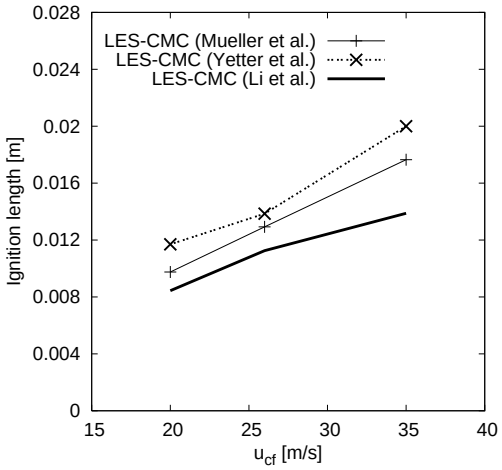

Fig. 13: Influence of co-flow velocity on the flame lift-off height ($T_{cf} = 960$K).